J. Fluid Mech. (1995), vol. 300, pp. 265–285

An instability in supersonic boundary-layer flow over a compression ramp

By K. W. CASSEL[1], A. I. RUBAN[2] AND J. D. A. WALKER[1]

[1]Department of Mechanical Engineering and Mechanics, Lehigh University, Bethlehem, PA 18015, USA

[2]Central Aerohydrodynamic Institute (TsAGI), Zhukovsky, Moscow Region, Russia

(Received 10 March 1995 and in revised form 26 May 1995)

Separation of a supersonic boundary layer (or equivalently a hypersonic boundary layer in a region of weak global interaction) near a compression ramp is considered for moderate wall temperatures. For small ramp angles, the flow in the vicinity of the ramp is described by the classical supersonic triple-deck structure governing a local viscous–inviscid interaction. The boundary layer is known to exhibit recirculating flow near the corner once the ramp angle exceeds a certain critical value. Here it is shown that above a second and larger critical ramp angle, the boundary-layer flow develops an instability. The instability appears to be associated with the occurrence of inflection points in the streamwise velocity profiles within the recirculation region and develops as a wave packet which remains stationary near the corner and grows in amplitude with time.

1. Introduction

Boundary-layer theory has provided a framework to investigate many aspects of flow at high Reynolds number, and one of the most interesting of these is separation. The boundary-layer equations are based on the premise that the viscous layer remains thin, with a thickness of $O(Re^{-1/2})$ in the limit of infinite Reynolds number Re. This generally implies that the normal velocity at the boundary-layer edge is small, thereby suggesting that the influence of the boundary layer on the external inviscid flow is small. However, when the mainstream pressure gradient is adverse, the low-momentum fluid adjacent to the surface is susceptible to the onset of reversed flow, which may lead to boundary-layer separation and a concomitant significant interaction with the outer inviscid flow.

A classical situation where viscous–inviscid interactions play a central role in the flow dynamics occurs when a shock wave impinges on a supersonic boundary layer. In several early experimental investigations (see, for example, Liepmann 1946; Ackeret, Feldmann & Rott 1947 and Chapman, Kuehn & Larsen 1957), the incident shock wave was observed to provoke boundary-layer separation upstream of the point of impingement of the primary shock, with a secondary shock forming near the separation point. This situation constitutes an example of a compressive disturbance wherein the disturbance (the shock wave) induces a rise in the inviscid pressure along the surface. A compressive disturbance in a supersonic flow may also be caused by a surface that turns toward the flow. In a series of experiments, Chapman *et al.* (1957) studied a variety of situations where separation was induced by such surface geome-

tries (including steps and corners) and where separation occurred invariably upstream of the disturbance. The upstream influence observed in these examples was perplexing at the time since: (i) the boundary-layer equations are parabolic and, therefore, do not permit upstream propagation of disturbances, and (ii) the supersonic external flow can only transmit disturbances downstream. The first theoretical explanation for the propagation of disturbances upstream was given by Lighthill (1953) in the context of a linear theory which is valid for disturbances of small amplitude; he argued that a compressive disturbance gives rise to an adverse mainstream pressure gradient, and once the disturbance is of sufficient strength, boundary-layer separation must occur. As a consequence, the boundary-layer thickness can act to alter the external flow by provoking a pressure rise ahead of the separation point, which in turn causes the flow to separate farther upstream. This phenomenon is often called self-induced separation.

The theoretical work of Lighthill (1953) formed the basis for the supersonic triple-deck theory of Stewartson & Williams (1969) and Neiland (1969) which included nonlinear effects and provided a theoretical explanation for the upstream influence, as well as for self-induced separation of a boundary layer in supersonic flow. Subsequently, triple-deck theory has been applied to many seemingly diverse problems throughout the subsonic, supersonic and hypersonic flow regimes. However, each problem contains a common feature in the form of some surface or mainstream disturbance, which acts to provoke a viscous–inviscid interaction in a local region where upstream influence is facilitated. Comprehensive descriptions of triple-deck problems appear in the reviews of Neiland (1974, 1981), Stewartson (1974, 1981), Messiter (1979, 1983), Adamson & Messiter (1980) and Smith (1982).

The triple-deck formulation was extended to the case of hypersonic flow by Neiland (1970) for small, finite and large values of the viscous hypersonic interaction parameter and then to three-dimensional motion by Kozlova & Mikhailov (1970). Analysis of hypersonic boundary-layer separation on a cold wall was carried out by Neiland (1973) and Brown, Cheng & Lee (1990), and for a special case of hypersonic flow (in which the specific heat ratio approaches one) by Brown, Stewartson & Williams (1975). In contrast to the abrupt change in flow characteristics from subsonic to supersonic flow at Mach 1, the transition from supersonic to hypersonic flow is not as clearly defined, but instead is characterized by new physical effects which gradually become more important as the mainstream Mach number M_∞ is increased. Hypersonic boundary layers generally grow much more rapidly than their supersonic counterparts owing to substantial viscous dissipation within the boundary layer; this results in significant increases in temperature that, in turn, both increase the viscosity coefficient and also decrease the gas density. Both effects combine to cause the boundary-layer thickness δ to grow rapidly. For example, if the viscosity is assumed to vary linearly with temperature, then the boundary layer thickens proportionately to $M_\infty^2 Re_x^{-1/2}$, where Re_x is the local Reynolds number along the surface. The rapid growth in δ can provoke a global interaction with the outer inviscid flow, which is generally strong near the leading edge of a body, but weakens further downstream, provided δ remains small in comparison to the body thickness. Further discussion of this global viscous interaction has been given by Anderson (1989), Mikhailov, Neiland & Sychev (1971) and Cheng (1993). The hypersonic triple-deck formulation considered here applies in regions of weak global viscous interaction, where the interaction is localized and due to some small-scale feature.

It has been shown by Neiland (1973), Brown *et al.* (1990) and Kerimbekov, Ruban & Walker (1994) that in a hypersonic triple deck, a sufficient level of wall cooling

can significantly alter the nature of the interaction with the external flow, and such situations have recently been considered by Cassel, Ruban & Walker (1995). However, when the wall temperature is comparable to the mainstream stagnation temperature and the viscous interaction parameter $\chi = M_\infty \delta \ll 1$, the triple-deck equations for hypersonic flow are the same as in the classical formulation described by Stewartson & Williams (1969) and Neiland (1969) for supersonic flow. Numerical solutions of this case have been obtained in the past by Rizzetta, Burggraf & Jenson (1978), Ruban (1978) and Smith & Khorrami (1991) for a boundary layer encountering a compression ramp defined by

$$f(x) = \begin{cases} 0, & x < 0, \\ \alpha x, & x > 0. \end{cases} \tag{1.1}$$

Here, x is a scaled streamwise distance, and α is the scaled ramp angle; the actual physical ramp angles considered are small and $O(Re^{-1/4})$. The numerical results of previous studies are generally all consistent for steady flow. These solutions exhibit a separation region anchored on the corner once the ramp angle exceeds a certain critical value. As the ramp angle is progressively increased, the extent of the recirculation region grows, and a plateau is observed to form in the predicted pressure distribution near the separation point.

In most interacting boundary-layer problems there is at least one controlling parameter; for surface humps on the wall, this parameter is the hump height, while it is the shock strength for shock-induced separation and the scaled angle α for the compression ramp. As the controlling parameter is increased, a continual increase in the streamwise extent of the separation region is generally observed. Many investigators have attempted to consider the transition from small-scale to large-scale separation in high Reynolds number flows by gradually increasing the value of α. Such attempts have in general been unsuccessful since severe numerical difficulties are invariably encountered once the reverse-flow regions reach an appreciable size. Smith (1988) has observed that many such calculations exhibit increasing maximums in the pressure gradient and decreasing negative minimums in the wall shear at some point x_0 between separation and reattachment as the controlling parameter is increased. Smith (1988) then showed that a singularity could occur in the solution of the steady interactive boundary-layer equations at some finite value $\alpha = \alpha_c$ at $x = x_0$. The flow in the immediate vicinity of the singularity is inviscid to leading order on a short streamwise length scale $(x - x_0) = O(\hat{\Delta})$, where $\hat{\Delta} = (\alpha_c - \alpha)^2$. The maximum in the pressure gradient $\mathrm{d}p/\mathrm{d}x$ and minimum in the wall shear τ_w are singular at x_0 as $\alpha \to \alpha_c$ and are of the form

$$\max\left(\frac{\mathrm{d}p}{\mathrm{d}x}\right) \sim \hat{\Delta}^{-1}, \quad \min(\tau_w) \sim -\hat{\Delta}^{-1/2}. \tag{1.2}$$

Smith & Khorrami (1991) carried out a series of calculations for steady flow past a compression ramp and estimated the critical value of α_c to be 'somewhat below 9'. The implication of the above results is that the triple-deck formulation fails for even moderate values of the controlling parameter and, consequently, asymptotic solutions for triple-deck theory cannot be constructed in the limit $\alpha \to \infty$. In order to relieve the reversed-flow singularity, Smith (1988) has argued that a narrow streamwise region must form locally about $x = x_0$ (having a streamwise extent $O(Re^{-5/8})$ for the triple-deck problem); here the inviscid Euler equations govern the motion and normal pressure gradient effects are conjectured to act to relieve the singularity.

In the present study, a further set of numerical solutions are obtained for the triple-deck problem for the compression ramp. The results pertain to both supersonic flow and hypersonic flow in regions of weak global interaction, since each problem reduces to the same triple-deck formulation. The present calculations differ from previous solutions in a number of respects. First, transformations are introduced to reduce the infinite streamwise domain of the lower deck to a finite domain, thereby removing any numerical errors associated with applying the upstream and downstream boundary conditions at finite values of x. Secondly, the transformations that are utilized permit a close packing of the mesh points in the physical space, both near the wall and in the corner of the compression ramp, where the recirculation region develops. The combination of the mesh sizes used and the finite-domain transformations make possible a significantly higher spatial resolution than has been possible in previous studies. The integrations were carried out by integrating the unsteady triple-deck equations through to the steady state. For coarse mesh sizes, it proved possible to perform the integrations smoothly and to reproduce the results of previous studies. However, as the mesh was progressively refined, an instability was found to occur for ramp angles in excess of $\alpha = 3.9$, in the form of a wave packet that develops and remains stationary near the corner. Further refinement of the mesh produced essentially the same results, suggesting that this instability is physical as opposed to numerical. The instability appears to be associated with the development of an inflection point in the velocity profiles within the backflow zone.

2. Governing equations

Consider the flow of an ideal compressible gas past a plate of length L, which is oriented parallel to a uniform flow of speed U_∞, density ρ_∞, enthalpy h_∞ and pressure p_∞. The specific heat ratio γ for gas is assumed constant. A second semi-infinite plate is joined to the end of the first plate and oriented at a small angle α' to the flow direction to form a compression corner on the upper surface of the composite body. Define flow variables such that lengths, velocities, pressure, density, enthalpy and absolute viscosity are made dimensionless with respect to L, U_∞, $\rho_\infty U_\infty^2$, ρ_∞, U_∞^2 and μ_o, respectively. Here, μ_o is the viscosity coefficient evaluated at a reference enthalpy of U_∞^2; this choice is convenient for high-speed flows and is characteristic of the viscosity in the boundary layer, as opposed to utilizing a viscosity based on the reference free-stream static temperature T_∞ which is often relatively small. The viscosity is taken to be a function of temperature alone and given by the power law

$$\mu' = (h')^n, \tag{2.1}$$

where n is a positive constant. Here, and throughout, the prime will be used to denote unscaled dimensionless variables. The Reynolds number and Mach number are defined by

$$Re_0 = \frac{\rho_\infty U_\infty L}{\mu_0}, \quad M_\infty = U_\infty \left(\frac{\gamma p_\infty}{\rho_\infty}\right)^{-1/2}, \tag{2.2a,b}$$

respectively. The Reynolds number is assumed large, while the Mach number is $O(1)$ for a supersonic external flow, and $M_\infty \to \infty$ in the hypersonic case. However, the hypersonic viscous interaction parameter

$$\chi = M_\infty^2 Re_0^{-1/2} \ll 1, \tag{2.3}$$

since the global viscous interaction is assumed to be weak and to have, therefore, a negligible effect on the boundary layer in the vicinity of the ramp. Note that Re_0 is defined here in terms of μ_0 rather than a viscosity coefficient μ_∞ evaluated at the mainstream static temperature (see, for example, Brown *et al.* 1990).

Let x' and y' be coordinates along and normal to the surface (with origin at the leading edge), respectively, with (u', v') denoting the corresponding velocity components; let p' be dimensionless pressure and t' be time. When the mainstream flow approaching the compression ramp is supersonic, the longitudinal velocity in the boundary layer is a function of x' and the scaled normal variable $\bar{y} = y' Re^{1/2}$, and with the approach to the corner is of the form

$$u' \to \lambda \bar{y} \quad \text{as} \quad x' \to 1, \quad \bar{y} \to 0. \tag{2.4}$$

Here λ is a constant whose value is $O(1)$ and is determined from the boundary-layer solution upstream of the corner. A triple deck develops in the corner region, and the lower-deck problem depends on the following scaled variables (see, for example, Rizzetta *et al.* 1978; Ruban 1978):

$$x' - 1 = \rho_w^{-1/2} \mu_w^{-1/4} \lambda^{-5/4} \beta^{-3/4} Re_0^{-3/8} x, \tag{2.5a}$$

$$y' = \rho_w^{-1/2} \mu_w^{1/4} \lambda^{-3/4} \beta^{-1/4} Re_0^{-5/8} (y - f(x)), \tag{2.5b}$$

$$u' = \rho_w^{-1/2} \mu_w^{1/4} \lambda^{1/4} \beta^{-1/4} Re_0^{-1/8} u(x, y, t), \tag{2.5c}$$

$$v' = \rho_w^{-1/2} \mu_w^{3/4} \lambda^{3/4} \beta^{1/4} Re_0^{-3/8} (v(x, y, t) - \mathrm{d}f/\mathrm{d}x) \tag{2.5d}$$

$$p' - 1 = \lambda^{1/2} \mu_w^{1/2} \beta^{-1/2} Re_0^{-1/4} p(x, t), \tag{2.5e}$$

$$t' = \lambda^{-3/2} \mu_w^{-1/2} \beta^{-1/2} Re_0^{-1/4} t. \tag{2.5f}$$

Here $\beta = (M_\infty^2 - 1)^{1/2}$ and β is $O(1)$ for supersonic flow; in addition, the surface contour is defined by $y = f(x)$, and a Prandtl transposition has been incorporated in equations (2.5). Values of λ, ρ_w and μ_w are assumed known, with ρ_w and μ_w being the dimensionless density and viscosity at the wall; for supersonic flow ρ_w is $O(1)$. The compression ramp angle (cf. equation (1.1)) is scaled according to

$$\alpha' = \lambda^{1/2} \mu_w^{1/2} \beta^{1/2} Re_0^{-1/4} \alpha, \tag{2.6}$$

where α is a prescribed $O(1)$ constant; the ramp angle α' in the physical space is therefore small in the limit $Re_0 \to \infty$.

Upon substitution in the Navier–Stokes and energy equations, it is easily shown that $\rho \equiv \rho_w$ and $\mu \equiv \mu_w$ in the lower deck, while (u, v, p) satisfy

$$\frac{\partial u}{\partial t} + u \frac{\partial u}{\partial x} + v \frac{\partial u}{\partial y} = -\frac{\partial p}{\partial x} + \frac{\partial^2 u}{\partial y^2}, \tag{2.7a}$$

$$\frac{\partial u}{\partial x} + \frac{\partial v}{\partial y} = 0, \tag{2.7b}$$

with boundary conditions

$$u = v = 0 \quad \text{at} \quad y = 0, \quad u \to y + A(x, t) + \ldots \quad \text{as} \quad y \to \infty, \tag{2.8}$$

and

$$u \to y \quad \text{as} \quad x \to -\infty, \tag{2.9}$$

where $A(x,t)$ represents the displacement thickness of the viscous sublayer. The interaction law is given by the Ackeret formula

$$p = -\frac{\partial A}{\partial x} + \frac{\partial f}{\partial x}, \tag{2.10}$$

which is obtained from analysis of the inviscid flow in the upper deck of the triple-deck structure.

With increasing mainstream Mach number, the density in the boundary layer decreases, and as $M_\infty \to \infty, \rho$ becomes $O(M_\infty^{-2})$ (see, for example, Stewartson 1964). For a hypersonic mainstream flow, therefore, a scaled density ρ may be defined in terms of the dimensionless (with respect to ρ_∞) density ρ', as well as a scaled normal coordinate $\bar{y}$ by

$$\rho = \rho' M_\infty^2, \quad \bar{y} = y' \frac{Re_0^{1/2}}{M_\infty}. \tag{2.11a,b}$$

In the boundary layer upstream of the corner, the solution is a function of $(x', \bar{y})$ and the longitudinal velocity u' satisfies equation (2.4) as the corner is approached, where again λ is an $O(1)$ constant. Let ρ_w denote the value of the density function defined by equation (2.11a) at the wall, with μ_w being the dimensionless viscosity at the wall. The scaled variables in the lower deck of the hypersonic triple deck may be obtained from equations (2.5) by replacing (ρ_w, β, λ) by $(\rho_w/M_\infty^2, M_\infty, \lambda/M_\infty)$, respectively. This has the net effect of replacing the factors of β in equations (2.5a)–(2.6) by $M_\infty^{3/2}$, $M_\infty^{3/2}$, $M_\infty^{1/2}$, $M_\infty^{1/2}$, M_∞^{-1}, M_∞^{-1} and 1, respectively. Upon substitution in the Navier–Stokes equations, it is then easily shown that $\rho' \equiv \rho_w/M_\infty^2$ and $\mu \equiv \mu_w$ in the lower deck, while (u,v,p) satisfy the generic triple-deck problem defined by equations (2.7)–(2.10).

The basic shear flow $u = y$ is known to be stable with respect to small-amplitude perturbations which are in a form consistent with equations (2.5), when both the basic flow and the perturbations may be described by equations (2.7)–(2.10). However as the motion evolves, the flow might take a form possibly containing a Rayleigh instability (Tutty & Cowley 1986). The occurrence of such instabilities was demonstrated numerically by Tutty & Cowley (1986) for an interaction law of the form $p = A$ and has also been found in the first interactive stage of unsteady separation (Peridier, Smith & Walker 1991; Cassel, Smith & Walker 1994). Denote the exact solution of the triple-deck problem (2.7)–(2.10) by subscript zero and assume that infinitesimal harmonic disturbances are introduced of the form

$$u = u_0(x,y,t) + \varepsilon e^{i(\alpha x - \alpha c t)} u_1(x,y,t) + ..., \tag{2.12a}$$

$$v = v_0(x,y,t) + \varepsilon e^{i(\alpha x - \alpha c t)} \alpha v_1(x,y,t) + ..., \tag{2.12b}$$

$$p = p_0(x,t) + \varepsilon e^{i(\alpha x - \alpha c t)} p_1(x,t) + ..., \tag{2.12c}$$

$$A = A_0(x,t) + \varepsilon e^{i(\alpha x - \alpha c t)} A_1(x,t) + ..., \tag{2.12d}$$

where $\varepsilon \ll 1, \alpha$ is real, and $c = c_r + ic_i$ is the complex wave speed. It is anticipated that a possible instability will be inviscid having short wavelengths (and therefore high frequencies) compared with the interaction length scales; thus the situation of interest corresponds to $\alpha \gg 1$. Tutty & Cowley (1986) show that a necessary and sufficient condition for instability of high-frequency perturbations is the eigenvalue relation

$$\int_0^\infty \frac{dy}{(u_0 - c)^2} = 0, \tag{2.13}$$

which serves to determine the complex wave speed c for a given streamwise velocity

profile u_0; in equation (2.13), the integral is across the boundary layer at fixed x. The flow is unstable to small disturbances if $c_i > 0$. As discussed by Tutty & Cowley (1986), Rayleigh's inflection point theorem and Fjøtoft's theorem are necessary conditions for an instability in situations where the eigenrelation is of the form given by equation (2.13). Rayleigh's theorem requires the existence of an inflection point in the velocity profile $u_0(x, y, t)$, and Fjørtoft's theorem states that a necessary condition for instability is that

$$\frac{\partial^2 u_0}{\partial y^2}\left[u_0(y) - u_0(y_{ip})\right] < 0 \tag{2.14}$$

somewhere in the flow field, where y_{ip} is the location of the inflection point. Both of these conditions are necessary, but not sufficient, for the occurrence of a high-frequency instability, whereas condition (2.13) is both necessary and sufficient.

3. Formulation

It is convenient to reformulate the triple-deck problem (2.7)–(2.10) in terms of the scaled shear stress $\tau = \partial u/\partial y$ since this permits elimination of both the pressure $p(x, t)$ from the momentum equation (2.7*a*) and displacement function $A(x, t)$ from the boundary condition (2.8). Differentiation of equation (2.7*a*) with respect to y eliminates p and leads to

$$\frac{\partial \tau}{\partial t} + u\frac{\partial \tau}{\partial x} + v\frac{\partial \tau}{\partial y} = \frac{\partial^2 \tau}{\partial y^2}. \tag{3.1}$$

The velocity components may be written in terms of a streamfunction defined by $u = \partial\psi/\partial y$, $v = -\partial\psi/\partial x$, and τ is related to ψ by

$$\frac{\partial^2 \psi}{\partial y^2} = \tau. \tag{3.2}$$

The boundary conditions associated with the system (3.1) and (3.2) are

$$\psi = \frac{\partial \psi}{\partial y} = 0 \quad \text{at} \quad y = 0, \tag{3.3}$$

$$\tau \to 1 \quad \text{as} \quad x \to \pm\infty \quad \text{and as} \quad y \to \infty. \tag{3.4}$$

Note that the condition (3.4) is also applied as $x \to +\infty$ because downstream of the local interaction, the flow is assumed to return to its upstream form. In the present study, numerical solutions were obtained by integrating the system (3.1)–(3.4) forward in time starting from

$$\tau = 1 \quad \text{at} \quad t = 0, \text{ for all } x \text{ and } y. \tag{3.5}$$

Next, consider the interaction condition (2.10). The displacement function A may be written as

$$A(x, t) = \lim_{y\to\infty}(u - y) = \lim_{y\to\infty}\int_0^y (\tau - 1)\mathrm{d}y. \tag{3.6}$$

Upon differentiating the interaction law (2.10) with respect to x and utilizing the result (from equation (2.7*a*) that

$$\frac{\partial p}{\partial x} = \left.\frac{\partial \tau}{\partial y}\right|_{y=0}, \tag{3.7}$$

it is easily shown that the interaction law (2.10) may be expressed solely in terms of

the shear stress and the known surface shape $f(x)$, namely

$$\left.\frac{\partial\tau}{\partial y}\right|_{y=0} = -\frac{\partial^2}{\partial x^2}\int_0^\infty (\tau - 1)\mathrm{d}y + \frac{\mathrm{d}^2 f}{\mathrm{d}x^2}. \tag{3.8}$$

For computational purposes, it proves convenient to transform the region $(-\infty, 0) \leqslant (x, y) \leqslant (\infty, \infty)$ into a finite rectangular domain by the transformations

$$\hat{x} = \frac{2}{\pi}\arctan\left(\frac{x}{a}\right), \quad \hat{y} = \frac{2}{\pi}\arctan\left(\frac{y}{b}\right), \tag{3.9a,b}$$

so that the computational domain is defined in $(-1, 0) \leqslant (\hat{x}, \hat{y}) \leqslant (1, 1)$. The parameters a and b determine the relative concentration of mesh points in (x, y)-space near the corner at $x = 0$ and the surface at $y = 0$, respectively. The transformation (3.9a) also eliminates the need to truncate the domain at some finite value of x upstream and downstream of the disturbance as has been done in previous studies (see, for example, Rizzetta *et al.* 1978; and Ruban 1978). It is easily shown that the system (3.1) and (3.2) transforms to

$$\frac{\partial\tau}{\partial t} + \frac{\Gamma(\hat{x})}{a}u\frac{\partial\tau}{\partial\hat{x}} + \frac{\Gamma(\hat{y})}{b}v\frac{\partial\tau}{\partial\hat{y}} = \frac{\Gamma(\hat{y})}{b}\frac{\Gamma'(\hat{y})}{b}\frac{\partial\tau}{\partial\hat{y}} + \frac{\Gamma^2(\hat{y})}{b^2}\frac{\partial^2\tau}{\partial\hat{y}^2}, \tag{3.10}$$

$$\frac{\Gamma(\hat{y})}{b}\frac{\partial}{\partial\hat{y}}\left[\frac{\Gamma(\hat{y})}{b}\frac{\partial\psi}{\partial\hat{y}}\right] = \tau, \tag{3.11}$$

where

$$\Gamma(\zeta) = \frac{1}{\pi}[1 + \cos(\pi\zeta)]. \tag{3.12}$$

The boundary conditions are

$$\tau \to 1 \quad \text{as} \quad \hat{x} \to \pm 1 \quad \text{and as} \quad \hat{y} \to 1, \tag{3.13}$$

$$\psi = \frac{\partial\psi}{\partial\hat{y}} = 0, \quad \text{at} \quad \hat{y} = 0, \tag{3.14}$$

while the interaction law (3.8) becomes

$$\left.\frac{\Gamma(0)}{b}\frac{\partial\tau}{\partial\hat{y}}\right|_{\hat{y}=0} = -\left[\frac{\Gamma(\hat{x})}{a}\frac{\Gamma'(\hat{x})}{a}\frac{\partial}{\partial\hat{x}} + \frac{\Gamma^2(\hat{x})}{a^2}\frac{\partial^2}{\partial\hat{x}^2}\right] b\int_0^1 \frac{\tau - 1}{\Gamma(\hat{y})}\mathrm{d}\hat{y} + \frac{\mathrm{d}^2 f}{\mathrm{d}x^2}. \tag{3.15}$$

Note that since $f(x)$ is a known function, the second derivative in equation (3.15) is conveniently left in terms of x. Finally, the velocity components are defined in terms of the streamfunction by

$$u = \frac{\Gamma(\hat{y})}{b}\frac{\partial\psi}{\partial\hat{y}}, \quad v = -\frac{\Gamma(\hat{x})}{a}\frac{\partial\psi}{\partial\hat{x}}. \tag{3.16a,b}$$

4. Numerical methods

Starting from the initial condition $u = y$, the solution for a given ramp angle was integrated forward in time until either a steady-state solution was reached or an instability was encountered. In this integration, a solution of the momentum equation (3.10) is required subject to the conditions (3.13) and the interaction law (3.15). At any stage, the streamfunction $\psi(\hat{x}, \hat{y}, t)$ and $u(\hat{x}, \hat{y}, t)$ were obtained by integrating equation (3.11) for a given estimate of τ subject to conditions (3.14); the solution for $v(\hat{x}, \hat{y}, t)$ is

then obtained by differentiation according to equation (3.16*b*). The implicit algorithm described below combines the momentum equation and the interaction law in such a manner that iteration between the boundary-layer solution and outer inviscid solution is not necessary at each time step. The algorithm is based on an approach due to Ruban (1978) and is also similar to that used by Rizzetta *et al.* (1978).

Although the computational domain is finite in $\hat{y}$, the streamwise velocity is of the form $u \sim y$ as $y \to \infty$, and it is necessary, therefore, to choose a finite value of y at which to truncate the vertical extent of the domain. Denote this value by $y_{\max}$ with the corresponding value $\hat{y}_{\max}$ obtained from equation (3.9*b*). The region $(-1, 0) \leqslant (\hat{x}, \hat{y}) \leqslant (1, \hat{y}_{\max})$ was then divided into $I-1$ and $J-1$ equal mesh lengths $\Delta\hat{x}$ and $\Delta\hat{y}$ in the $\hat{x}$- and $\hat{y}$-directions, respectively. Quantities, such as $\tau(\hat{x}, \hat{y}, t)$, at the point $(\hat{x}_i, \hat{y}_j)$ are denoted by $\tau_{i,j}$ at the current time step where the solution is sought; the corresponding values at the previous time step where the solution is known are denoted by an asterisk, i.e. $\tau^*_{i,j}$. The following difference equation was used to approximate equation (3.10):

$$\frac{\tau_{i,j}-\tau^*_{i,j}}{\Delta t}+\frac{\Gamma(\hat{x}_i)}{a}\left(u\frac{\partial\tau}{\partial\hat{x}}\right)^*_{i,j}+\frac{\Gamma(\hat{y}_j)}{b}v^*_{i,j}\left(\frac{\tau_{i,j+1}-\tau_{i,j-1}}{2\Delta\hat{y}}\right)$$
$$=\frac{\Gamma(\hat{y}_j)}{b}\frac{\Gamma'(\hat{y}_j)}{b}\left(\frac{\tau_{i,j+1}-\tau_{i,j-1}}{2\Delta\hat{y}}\right)+\frac{\Gamma^2(\hat{y}_j)}{b^2}\left(\frac{\tau_{i,j+1}-2\tau_{i,j}+\tau_{i,j-1}}{(\Delta\hat{y})^2}\right), \tag{4.1}$$

for $i = 2, ..., I-1$ and $j = 2, ..., J-1$. It may be noted that the streamwise convective term and the normal velocity are evaluated at the previous time step as shown. In equation (4.1) conventional central differences are used in the direction normal to the wall, while the streamwise convection term is approximated by a second-order-accurate (in $\Delta\hat{x}$) backward or forward difference depending on the sign of $u^*_{i,j}$ as follows:

$$\left(u\frac{\partial\tau}{\partial\hat{x}}\right)^*_{i,j}=\begin{cases} u^*_{i,j}\dfrac{3\tau^*_{i,j}-4\tau^*_{i-1,j}+\tau^*_{i-2,j}}{2\Delta\hat{x}} & \text{for } u^*_{i,j}\geqslant 0, \\ -u^*_{i,j}\dfrac{3\tau^*_{i,j}-4\tau^*_{i+1,j}+\tau^*_{i+2,j}}{2\Delta\hat{x}} & \text{for } u^*_{i,j}<0. \end{cases} \tag{4.2}$$

It is evident that all spatial approximations are second-order accurate, while the algorithm is first-order accurate in time.

Equation (4.1) defines the tridiagonal problem for $\tau_{i,j}$ at each $\hat{x}_i$, for $i = 2, ..., I-1$, which is of the form

$$c^-_j\tau_{i,j-1}+c_j\tau_{i,j}+c^+_j\tau_{i,j+1}=d_j, \quad j=2,...,J-1, \tag{4.3}$$

where

$$c_j=-2A-\frac{1}{\Delta t}, \tag{4.4a}$$

$$c^-_j=A-\frac{\Gamma(\hat{y}_j)}{2b\Delta\hat{y}}\left\{\frac{\Gamma'(\hat{y}_j)}{b}-v^*_{i,j}\right\}, \tag{4.4b}$$

$$c^+_j=2A-c^-_j, \tag{4.4c}$$

$$d_j=\frac{\Gamma(\hat{x}_i)}{a}\left(u\frac{\partial\tau}{\partial\hat{x}}\right)^*_{i,j}-\frac{\tau^*_{i,j}}{\Delta t}, \tag{4.4d}$$

where $A = \Gamma^2(\hat{y}_j)/(b\Delta\hat{y})^2$. The solution of the difference equations (4.3) can be

expressed in the form

$$\tau_{i,j} = R_j \tau_{i,j-1} + Q_j, \quad j = 2, ..., J, \tag{4.5}$$

where to satisfy condition (3.13) at $j = J$

$$R_J = 0, \quad Q_J = 1, \tag{4.6a,b}$$

and for $j = J-1, ..., 2$

$$R_j = -\frac{c_j^-}{c_j + c_j^+ R_{j+1}}, \quad Q_j = -\frac{c_j^+ Q_{j+1} - d_j}{c_j + c_j^+ R_{j+1}}. \tag{4.7a,b}$$

Note that these relations are essentially an elimination procedure similar to the Thomas algorithm, with equations (4.7) constituting a recursive calculation to evaluate the coefficients R_j and Q_j starting at the boundary-layer edge and moving toward the wall. The back-substitution portion of the algorithm in equation (4.5) is a recursive formula to evaluate the shear stress $\tau_{i,j}$ at the ith station starting from the wall and moving toward the boundary-layer edge. Note that the difference equations are linear and that equation (4.5) expresses $\tau_{i,j}$ in terms of the value at the mesh point immediately below, i.e. $\tau_{i,j-1}$. Using these relations, the shear stress at any $\hat{y}_j$ for given $\hat{x}_i$ may conveniently be expressed in terms of the wall shear stress $\tau_{i,1}$ at that station, and it is easily shown that

$$\tau_{i,j} = C_{i,j} \tau_{i,1} + B_{i,j}, \quad j = 1, ..., J, \tag{4.8}$$

where

$$C_{i,1} = 1, \quad B_{i,1} = 0, \tag{4.9a,b}$$

$$C_{i,j} = R_j C_{i,j-1}, \quad B_{i,j} = R_j B_{i,j-1} + Q_j, \quad j = 2, ..., J, \tag{4.10a,b}$$

where R_j and Q_j are defined by equations (4.7). It is evident that the solution to the momentum equation for $\tau_{i,j}$ is known throughout the domain once the wall shear stress $\tau_{i,1}$is found.

In order to determine the wall shear stress, consider the interaction law (3.15). The integral in equation (3.15) may be approximated using the trapezoidal rule to give

$$b \int_0^{\hat{y}_{\max}} \frac{\tau - 1}{\Gamma(\hat{y})} d\hat{y} = \sum_{j=2}^{J} \frac{\Delta \hat{y}}{2} \left[\frac{b}{\Gamma(\hat{y}_j)} (\tau_{i,j} - 1) + \frac{b}{\Gamma(\hat{y}_{j-1})} (\tau_{i,j-1} - 1) \right]. \tag{4.11}$$

Substitution of equation (4.8) into equation (4.11) gives an expression for the integral which again is in terms of the wall shear, namely

$$b \int_0^{\hat{y}_{\max}} \frac{\tau - 1}{\Gamma(\hat{y})} d\hat{y} = N_i \tau_{i,1} + M_i, \tag{4.12}$$

where

$$N_i = \sum_{j=2}^{J} \frac{\Delta \hat{y}}{2} \left[\frac{b}{\Gamma(\hat{y}_j)} C_{i,j} + \frac{b}{\Gamma(\hat{y}_{j-1})} C_{i,j-1} \right], \tag{4.13a}$$

$$M_i = \sum_{j=2}^{J} \frac{\Delta \hat{y}}{2} \left[\frac{b}{\Gamma(\hat{y}_j)} (B_{i,j} - 1) + \frac{b}{\Gamma(\hat{y}_{j-1})} (B_{i,j-1} - 1) \right]. \tag{4.13b}$$

Similarly, approximating $\partial \tau / \partial \hat{y}$ at $\hat{y} = 0$ in equation (3.15) by a second-order-accurate

forward difference and utilizing equations (4.8) and (4.9) yields

$$\left.\frac{\partial\tau}{\partial\hat{y}}\right|_{\hat{y}=0} = \frac{4C_{i,2} - 3 - C_{i,3}}{2\Delta\hat{y}}\tau_{i,1} + \frac{4B_{i,2} - B_{i,3}}{2\Delta\hat{y}}. \tag{4.14}$$

Finally, substitution of equations (4.13) and (4.14) into (3.15), along with standard second-order central difference approximations for the derivatives of $\tau_{i,1}$ with respect to $\hat{x}$, yields the following tridiagonal system for the wall shear stress:

$$\bar{c}_i^{-}\tau_{i-1,1} + \bar{c}_i\tau_{i,1} + \bar{c}_i^{+}\tau_{i+1,1} = \bar{d}_i, \quad i = 2, ..., I-1, \tag{4.15}$$

where

$$\bar{c}_i = \frac{\Gamma^2(\hat{x}_i)}{a^2}\frac{2N_i}{(\Delta\hat{x})^2} - \frac{\Gamma(0)}{b}\left(\frac{4C_{i,2} - 3 - C_{i,3}}{2\Delta\hat{y}}\right), \tag{4.16a}$$

$$\bar{c}_i^{-} = -\frac{\Gamma^2(\hat{x}_i)}{a^2}\frac{N_{i-1}}{(\Delta\hat{x})^2} + \frac{\Gamma(\hat{x}_i)\Gamma'(\hat{x}_i)}{a^2}\frac{N_{i-1}}{2\Delta\hat{x}}, \tag{4.16b}$$

$$\bar{c}_i^{+} = -\frac{\Gamma^2(\hat{x}_i)}{a^2}\frac{N_{i+1}}{(\Delta\hat{x})^2} - \frac{\Gamma(\hat{x}_i)\Gamma'(\hat{x}_i)}{a^2}\frac{N_{i+1}}{2\Delta\hat{x}}, \tag{4.16c}$$

$$\bar{d}_i = \frac{\Gamma^2(\hat{x}_i)}{a^2}\left(\frac{M_{i+1} - 2M_i + M_{i-1}}{(\Delta\hat{x})^2}\right) + \frac{\Gamma(\hat{x}_i)\Gamma'(\hat{x}_i)}{a^2}\left(\frac{M_{i+1} - M_{i-1}}{2\Delta\hat{x}}\right) - \left.\frac{\mathrm{d}^2 f}{\mathrm{d}x^2}\right|_{x=x_i} + \frac{\Gamma(0)}{b}\left(\frac{4B_{i,2} - B_{i,3}}{2\Delta\hat{y}}\right). \tag{4.16d}$$

The tridiagonal system (4.15) was solved for the wall shear $\tau_{i,1}$ using the Thomas algorithm subject to conditions (3.13) which give

$$\tau_{1,1} = \tau_{I,1} = 1. \tag{4.17}$$

The shear stress throughout the domain was then computed from equation (4.8) for $i = 2, ..., I-1$; note that at the streamwise boundaries $\tau_{1,j} = \tau_{I,j} = 1$, $j = 2, ..., J$.

To calculate the velocity components at each time step, equation (3.16*a*) was first integrated to obtain the streamfunction throughout the domain according to the two integrations

$$u = b\int_0^{\hat{y}} \frac{\tau}{\Gamma(\hat{y})}\mathrm{d}\hat{y}, \quad \psi = b\int_0^{\hat{y}} \frac{u}{\Gamma(\hat{y})}\mathrm{d}\hat{y}, \tag{4.18a,b}$$

which were carried out using the trapezoidal rule starting from $u_{i,1} = \psi_{i,1} = 0$. The velocity v was then obtained using a second-order central difference in equation (3.16*b*).

A direct determination of the pressure distribution is not necessary for continuation of the present unsteady calculation; however, the pressure is of physical interest and may be computed at any desired time from the shear stress at the wall as follows. Substitution of equation (3.6) with equation (3.9*a*) into the interaction law (2.10) gives

$$p = \frac{\mathrm{d}f}{\mathrm{d}x} - \frac{\Gamma(\hat{x})}{a}\frac{\partial}{\partial\hat{x}}\left[b\int_0^{\hat{y}_{\max}} \frac{\tau - 1}{\Gamma(\hat{y})}\mathrm{d}\hat{y}\right]. \tag{4.19}$$

Substitution of equation (4.12) for the integral yields

$$p_i = \left.\frac{\mathrm{d}f}{\mathrm{d}x}\right|_i - \frac{\Gamma(\hat{x}_i)}{a}\left(\frac{N_{i+1}\tau_{i+1,1} + M_{i+1} - N_{i-1}\tau_{i-1,1} - M_{i-1}}{2\Delta\hat{x}}\right). \tag{4.20}$$

The boundary conditions for a general surface shape $f(x)$ are

$$p_1 = \left.\frac{\mathrm{d}f}{\mathrm{d}x}\right|_{x\to-\infty}, \quad p_I = \left.\frac{\mathrm{d}f}{\mathrm{d}x}\right|_{x\to+\infty}, \tag{4.21}$$

which for the compression ramp become $p_1 = 0$, $p_I = \alpha$, where α is the scaled ramp angle.

Stability of the above numerical algorithm requires that the Courant–Friedrichs–Lewy criterion, modified owing to the finite-domain transformations (3.9), be satisfied; this condition is $\Delta t \leqslant a\Delta\hat{x}/(2\,|\Gamma u|_{\max})$ where $|\Gamma u|_{\max}$ denotes the maximum value of $|\Gamma(\hat{x})u|$. From the definition (3.12) of Γ, the maximum value of Γ is $2/\pi$ which occurs when $\hat{x} = 0$; therefore, the stability criterion may be written as

$$\Delta t \leqslant \frac{\pi a \Delta\hat{x}}{4\,|u_{\max}|}. \tag{4.22}$$

Since $u \sim y + A$ as $y \to \infty$, the maximum streamwise velocity is achieved in the computational domain at $y_{\max}$ where the domain is truncated. The stability condition (4.22) evidently restricts the time step for a given choice of the streamwise mesh size $\Delta\hat{x}$. In the present calculations, the time step was restricted to values at least one-half of that indicated by the criterion (4.22) to ensure stability of the numerical algorithm.

5. Calculated results

As shown in equation (4.16*d*), the surface shape $f(x)$ enters the numerical algorithm as a second derivative with respect to x, and when the slope of $f(x)$ is discontinuous (as in equation (1.1)), the second derivative of $f(x)$ contains a delta function, thereby necessitating special treatment at the corner (see Rizzetta *et al.* 1978; and Brown *et al.* 1990). In order to keep the present algorithm general for various surface shapes $f(x)$, the corner was rounded slightly so that $\mathrm{d}^2f/\mathrm{d}x^2$ is a smooth function everywhere. In the present study, the surface shape was defined by

$$f(x) = \tfrac{1}{2}\alpha\left[x + (x^2 + r^2)^{1/2}\right], \tag{5.1}$$

instead of equation (1.1), where α is the scaled downstream ramp angle. Here, r is called the rounding parameter, and as $r \to 0$ the surface collapses to the sharp compression ramp. All subsequent results shown are for $r = 0.5$, although calculations were also carried out for other values. This particular value was found to eliminate numerical difficulties associated with the corner while at the same time minimizing the effect on the overall results. In general, the value of r has a significant influence on the ramp angle α at which separation first occurs; however, once separation occurs the flow development is essentially similar for all small values of r.

As discussed in §4, a finite value of $y_{\max}$ must be chosen at which to terminate the vertical extent of the computational domain. Numerical experimentation revealed that the solution was rather insensitive to the value of $y_{\max}$. For example, for a scaled ramp angle of $\alpha = 2.5$, there was no noticeable change in solutions having $y_{\max} \geqslant 10$. However, due to the transformation (3.9*b*) used for the y-coordinate, there is little advantage in minimizing $y_{\max}$ as was necessary in previous studies (see, for example, Rizzetta *et al.* 1978). Therefore, $y_{\max} = 50$ was used throughout, and the transformed $\hat{y}$-coordinate was discretized by defining a uniform mesh over the range $0 \leqslant \hat{y} \leqslant \hat{y}_{\max}$, where $\hat{y}_{\max}$ is related to $y_{\max}$ by equation (3.9*b*). Note, however, that the choice of $y_{\max}$ does affect the maximum time step which may be used as specified by the numerical stability criterion (4.22).

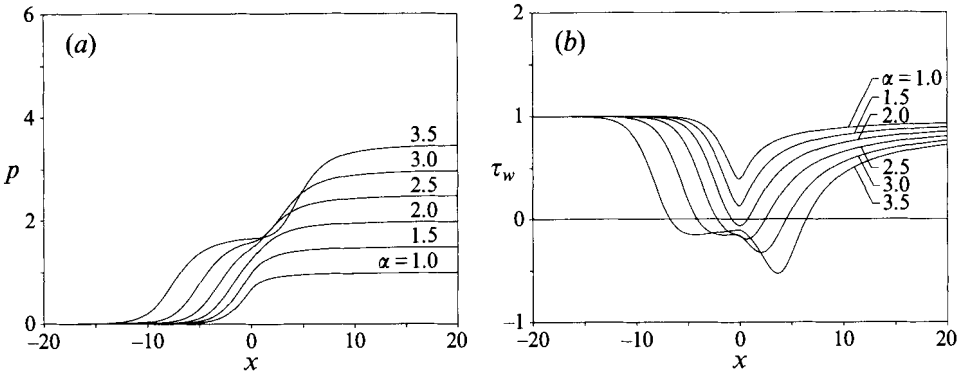

FIGURE 1. Numerical solutions for various small ramp angles α and $a = b = 5.0$: $I = 101$, $J = 51$ for $\alpha = 1.0, 1.5$; $I = 201$, $J = 101$ for $\alpha = 2.0, 2.5, 3.0, 3.5$. (*a*) Pressure, (*b*) wall shear stress.

Here, steady-state solutions for various parameters were sought as the large-time limit of unsteady calculations. The initial condition was taken to be $u = y$ corresponding to a flat plate ($\alpha = 0$), and at $t = 0$ the ramp angle was impulsively adjusted to its final value. The computation was marched forward in time until a steady state was reached. The unsteady numerical calculation was terminated at some large time at which $\partial\tau/\partial t$ (computed using a first-order backward difference) decreased below a given tolerance value at each mesh point along the wall; the tolerance was less than 5×10^{-4} in all cases. This tolerance was achieved for $\alpha = 3.5$ at approximately $t = 180$, for example, and at earlier times for smaller α.

Calculated pressure and wall shear distributions for a range of small ramp angles are shown in figures 1(*a*) and 1(*b*), respectively. Calculations were carried out for a number of mesh sizes, and the results shown are believed to be grid independent. In this and subsequent figures, the smallest mesh sizes used are shown in the captions along with the stretching factors a and b in the transformations (3.9); note that smaller values of a and b mean that in physical space progressively more mesh points are packed near the corner and wall, respectively. The pressure approaches zero as $x \to -\infty$ and tends smoothly to the reduced ramp angle α as $x \to \infty$. Likewise, the scaled wall shear tends to unity as $|x| \to \infty$. Reversed flow occurs adjacent to the surface when the wall shear becomes negative, and Rizzetta *et al.* (1978) estimated that this first occurs for $\alpha = 1.57$. In the present geometry, where the corner is rounded, separation first occurs at a slightly higher ramp angle of $\alpha = 1.9$ (to two significant figures). As the ramp angle is increased, the recirculating-flow region grows in extent as shown in figure 2, where the streamlines for several cases involving separation ($\alpha = 2.0, 2.5, 3.0, 3.5$) are shown; in addition, a constant-pressure plateau forms in the pressure distribution in the centre of the recirculation zone. The separation point moves progressively upstream with increasing α, while the point of reattachment moves increasingly downstream. Burggraf (1975) has given an estimate of the length of the separated-flow region based on a theory valid for large α. It may be noted that the movement of the reattachment point appears exaggerated in figure 2 because the stretched variable $y + f(x)$ is used; the actual streamwise extent of the separation zone is more accurately reflected in figure 1(*b*).

The present results *for small ramp angles* are in good agreement with results obtained in previous investigations and compare well with the results of Rizzetta *et al.* (1978) for $\alpha \leqslant 2.5$. For larger ramp angles, however, the present results exhibit a

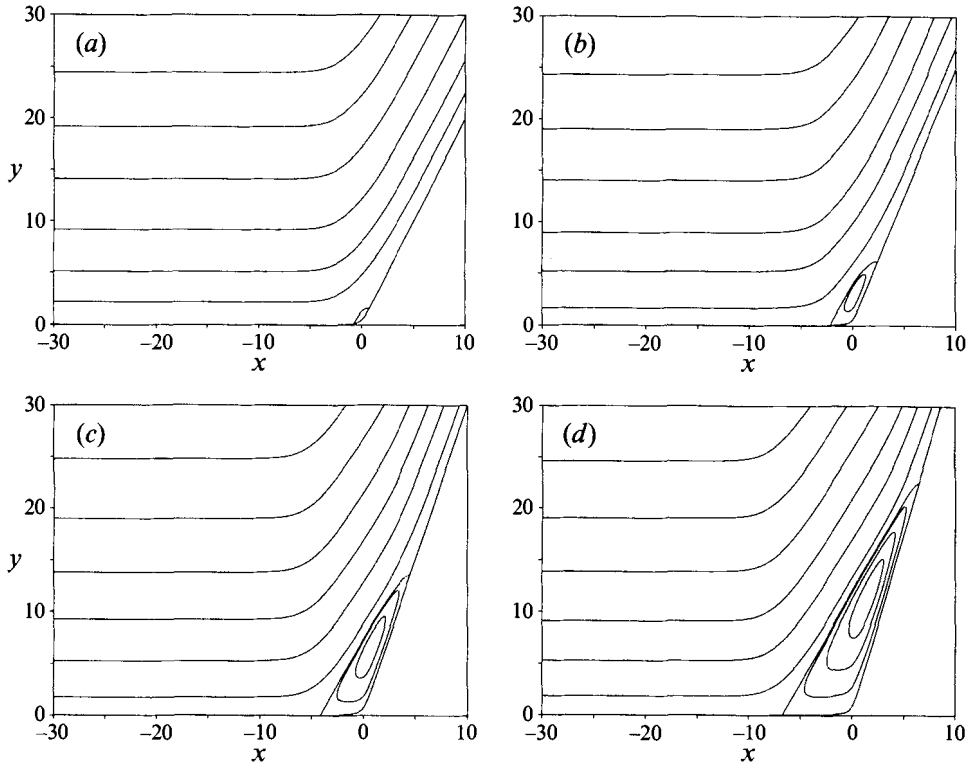

FIGURE 2. Streamlines for small ramp angles for $I = 201$, $J = 101$ and $a = b = 5.0$. (*a*) $\alpha = 2$, (*b*) $\alpha = 2.5$, (*c*) $\alpha = 3$, (*d*) $\alpha = 3.5$.

reversed-flow region with smaller streamwise and normal extent than that observed by Rizzetta *et al.* (1978), and are in closer agreement with the calculations of Ruban (1978) for $\alpha = 3.0$ and Smith & Khorrami (1991) for $\alpha = 3.5$. It should be noted that for even the coarsest mesh used in the present study with $I = 101$ and $J = 51$, the mesh sizes near the corner are at least half the size of those used in all previous studies. Rizzetta *et al.* (1978) also showed that the triple-deck solutions agree well with the experimental results of Lewis, Kubota & Lees (1968), and that they provide the limiting case for finite Reynolds number interacting-boundary-layer theory (see also Burggraf *et al.* 1979).

For cases involving separation, the rise in pressure and the drop in wall shear from the corresponding upstream values each have invariant shape as the ramp angle is increased, when plotted with origin at the separation point where $\tau_w = 0$. This corresponds to the free interaction considered experimentally by Chapman *et al.* (1957) and theoretically by Stewartson & Williams (1969). Increasing the strength of the disturbance (in this case the angle of the compression ramp) beyond a certain level does not change the flow approaching the reversed-flow region except to shift the separation point upstream. This was clearly illustrated in the numerical solutions obtained by Ruban (1978) who plotted the results for several cases involving separation with origin at the separation point.

The steady solutions obtained by Smith & Khorrami (1991) for larger ramp angles ($\alpha \geqslant 3.5$) show a continuation of the trends observed at lower ramp angles. As observed in figure 1(*b*), the minimum in wall shear drops below zero with

increasing ramp angle, and eventually the wall shear at the corner ($x = 0$) begins to rise as the ramp angle is increased above $\alpha = 3.0$ in apparent anticipation of an eventual secondary separation at the corner. Indeed, the numerical results of Smith & Khorrami (1991) actually show secondary separation ($\tau_w > 0$) at the corner for $\alpha \geqslant 4.5$, with a corresponding drop in pressure just downstream of the pressure plateau, prior to a subsequent rise to the downstream ramp pressure. As the ramp angle is increased further, their results show that a pronounced decrease in the wall shear minimum and increase in the pressure gradient maximum occur just upstream of the reattachment point. Smith & Khorrami (1991) showed that for steady flow, the wall shear and pressure gradient become singular at some large α in a manner previously determined by Smith (1988).

The present results, however, suggest that for large ramp angles the unsteady flow experiences an absolute instability in the form of a wave packet but at ramp angles well below the larger angles considered by Smith & Khorrami (1991). As discussed in §2, satisfaction of the Rayleigh and Fjørtoft criteria are necessary conditions for the occurrence of a high-frequency instability. Both criteria are satisfied when a velocity profile develops an inflection point such that the curvature of the velocity profile $\partial^2 u/\partial y^2$ is negative below the inflection point and positive above it. In the present calculations, it was found that the flow field is free of inflectional streamwise velocity profiles for $\alpha < 3.9$ (to two significant figures) but that inflection points first form for $\alpha = 3.9$ near the surface and immediately downstream of the corner. The critical value of $\alpha = 3.9$ was determined by evaluating $\partial^2 u/\partial y^2$, using a second-order central difference, from the steady solutions for various ramp angles. As the ramp angle is increased (at least up to $\alpha = 5.0$), the inflection point was found to move away from the surface, and there is an expanding streamwise range near $\hat{x} = 0$ over which streamwise inflectional profiles appear.

Because the presence of an instability was suspected for $\alpha \geqslant 3.9$, a series of calculations was carried out, and it was found that for sufficiently refined spatial grids, the numerical solutions did indeed become unstable for $\alpha \geqslant 3.9$ at the streamwise location where the velocity profiles were inflectional. Streamwise velocity profiles are shown at the corner ($x = 0$) for three different ramp angles ($\alpha = 3.5, 3.9$ and 4.5) in figure 3. Here, coarse meshes ($I = 101, J = 51$) were used for $\alpha = 3.9$ and 4.5 in order to suppress the instability. The velocity profile for $\alpha = 3.5$ shows that reversed flow can occur in the corner of the compression ramp without the appearance of inflection points. This is in contrast to the hump geometries considered by Kazakov (1985), Duck (1985) and Tutty & Cowley (1986), for which triple-deck solutions were found (using various interaction conditions) describing the flow over smooth humps of various heights where separation occurs on the downstream side of the hump for sufficiently large hump heights; however, in such cases, inflection points were found to appear in the streamwise velocity profiles for hump heights smaller than that necessary for reversed flow. It may be noted from figure 3 that as the ramp angle is increased, the magnitude of the reversed-flow velocity adjacent to the surface first decreases, and the lower portion of the velocity profile straightens out prior to formation of an inflection point. For $\alpha = 3.9$ the inflection point near $y = 0$ (from evaluation of $\partial^2 u/\partial y^2$) is not detectable graphically, while for $\alpha = 4.5$, the inflection point has moved away from the surface and is clearly visible.

In order to further confirm the existence of a physical instability, attempts were made to compute the eigenrelation (2.13) using the algorithm given by Tutty & Cowley (1986) (see also Cassel *et al.* 1995). It proved difficult, however, to find $O(1)$ values of the complex wave speed c which were clearly unstable for the ramp angles

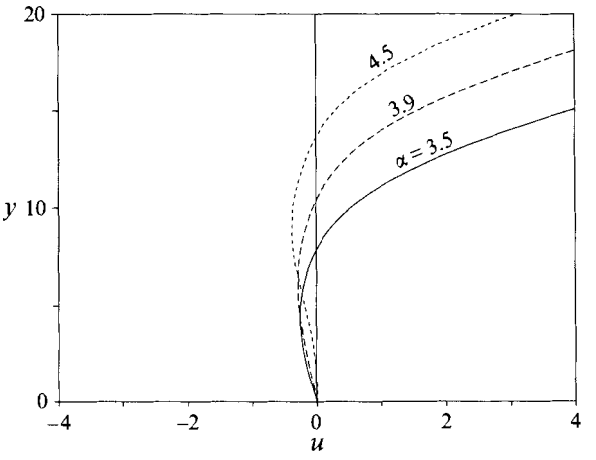

FIGURE 3. Streamwise velocity profiles at $x = 0$ for $\alpha = 3.5$ (——), $\alpha = 3.9$ (- - - - - - -) and $\alpha = 4.5$ (· · · · · · ·).

considered. In order to test the algorithm used for evaluating the integral in (2.13), the flow over the hump considered by Tutty & Cowley (1986) was recomputed for the surface geometry defined by $f(x) = he^{-10x^2}$, but using the supersonic interaction condition $p = -\partial A/\partial x$ rather than the interaction condition $A = 0$ used by Tutty & Cowley (1986). Results for Re(c) and Im(c) for a hump of height $h = 2$ were given by Tutty & Cowley (1986) (see their figure 2a), where c was found using a secant method and from evaluation of the instability criterion (2.13) for velocity profiles over a range of x; for this situation both Re(c) and Im(c) are $O(1)$, and essentially similar results were reproduced using the present codes that incorporate the supersonic Ackeret formula. However, for smaller hump heights close to the critical value at which Tutty & Cowley (1986) first found the flow to become unstable, it proved difficult to precisely determine c. In such cases, Im(c) is small and the streamwise range of unstable profiles is much shorter. Therefore, it is believed that for the compression ramp, Im(c), and thus the growth rate, is small for the ramp angles considered and is therefore difficult to determine from integration of equation (2.13). A contributing factor to the problems encountered in determining the eigenvalues of equation (2.13) may also be associated with the difference in the normal location of the inflection point in velocity profiles from the compression ramp and hump geometries; the inflection point is closer to the wall in the compression ramp case.

The observed instability for $\alpha \geqslant 3.9$ is manifest in the form of a wave packet which develops in the unsteady solution and remains stationary near the corner. A typical example is shown in figures 4 and 5, where a and b have been increased to 10.0 in order to ensure that the time step is sufficiently small to avoid instability of the numerical algorithm according to equation (4.22). Figure 4 shows the pressure and wall shear distributions after the instability has developed for a case with $\alpha = 4.0$, and figure 5 shows the temporal development of the wave packet for the same case. For $\alpha \geqslant 3.9$ the general form of the wave packet and its streamwise location remain the same, and the results shown are representative of those for all other ramp angles. The effect of mesh size on the instability is similar to that observed by Tutty & Cowley (1986) and Cassel *et al.* (1995), in that sufficient resolution is required in order to reveal the instability in the numerical calculations. This is presumably why the instability has not been observed in previous investigations of unsteady flow over compression ramps.

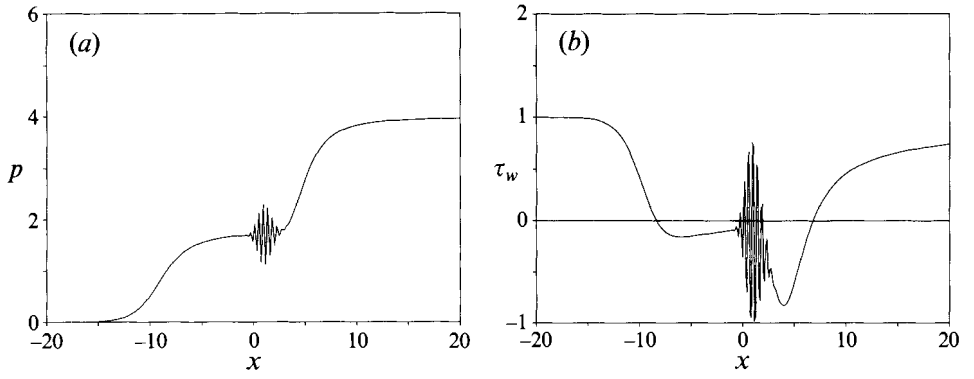

FIGURE 4. Stationary wave packet for $\alpha = 4.0$ at $t = 85.0$ with $I = 301$, $J = 151$ and $a = b = 10.0$. (*a*) Pressure, (*b*) wall shear stress.

Even in the present study, where the transformations (3.9) were used to concentrate grid points near the corner, no instability was observed in the numerical solutions for $3.9 \leqslant \alpha \leqslant 5.0$ when $I = 101$ and $J = 51$ were used. In these cases, the present results reached an apparent steady state and were in good agreement with those of Smith & Khorrami (1991). As the mesh was reduced, smaller-wavelength faster-growing unstable modes were admitted, and the small numerical errors introduced in the calculation were magnified causing the instability to form. For even finer meshes, the instability occurred at earlier times and evolved more rapidly owing to the faster growth rates. For example, the case shown in figures 4 and 5 computed with $I = 301$ and $J = 151$ revealed an instability at approximately $t = 85$, while the same case computed with $I = 201$ and $J = 101$ became unstable at about $t = 128$. The oscillations in figures 4 and 5 are basically point to point in the numerical mesh, and finer meshes produce smaller-scale oscillations. In addition, reductions in time step were found to delay, but not eliminate, the onset of the instability. Although changes in the spatial mesh and time step alter the time at which the instability forms, the streamwise extent and shape of the envelope surrounding the wave packet was found to be unaltered. In general, smaller spatial mesh sizes result in higher-frequency oscillations which are contained within an envelope of essentially the same shape.

6. Discussion

It has been shown that the supersonic flow or hypersonic flow (in regions of weak global interaction) over compression ramps on the triple-deck scales is unstable in the form of stationary wave packets that develop for ramp angles above a critical value. It follows from a linear stability analysis that Rayleigh's and Fjørtoft's criteria are necessary conditions for instability associated with high-frequency disturbances. These criteria require the formation of an inflection point in a velocity profile such that the curvature is negative below the inflection point and positive above it. In addition, a stability condition is known which provides a necessary and sufficient criterion for the occurrence of high-frequency instabilities, but the eigenvalue relation proved difficult to accurately evaluate numerically for the flow over the compression ramp.

The results for small ramp angles ($\alpha \leqslant 3.5$) were in good agreement with previous studies which show that separation occurs in the corner once a critical ramp angle is exceeded. As the ramp angle is increased, the streamwise and normal extent of the

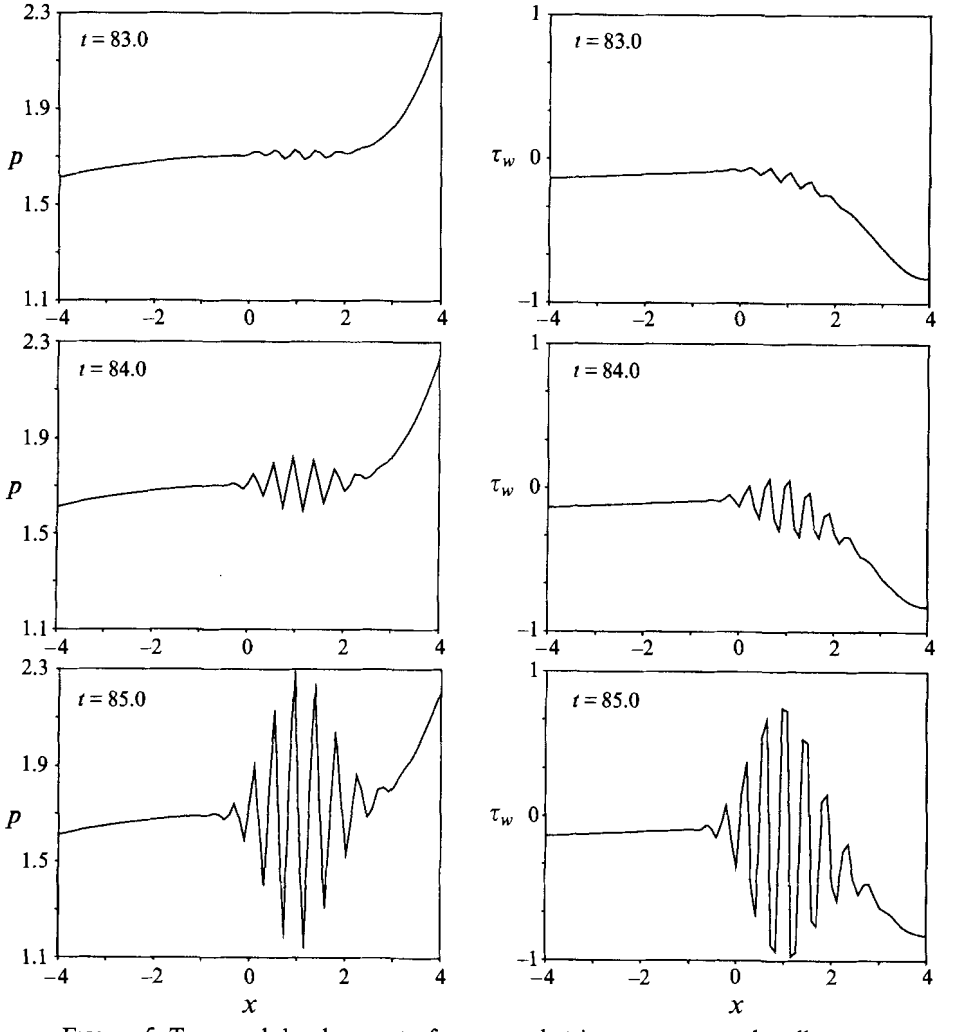

FIGURE 5. Temporal development of wave packet in pressure p and wall stress τ_w (same case as in figure 4).

recirculating-flow region grows substantially, and the pressure distribution develops a pressure plateau. As the ramp angle is increased further, it was found in the present study that a high-frequency absolute instability develops in the numerical solution in the form of a wave packet which remains stationary near the corner. This was found to occur for $\alpha \geqslant 3.9$ when sufficiently refined grids were used. The instability has high frequencies and short wavelengths, and for this reason it is highly mesh dependent. As the mesh is reduced, smaller-wavelength faster-growing modes were manifest in the calculation, and the instability appeared earlier in the unsteady calculation and grew more rapidly. While the specific form of the instability and the time at which it appears is highly mesh dependent, the bounding envelope of the wave packet maintained the same shape and streamwise extent regardless of the mesh used. In addition, the form of the wave packet remains largely the same for all ramp angles considered in which the flow became unstable. The existence of the instability in the numerical calculations is consistent with Rayleigh's and Fjørtoft's criteria. For $\alpha \leqslant 3.8$, the flow was found to contain no inflection points in the streamwise velocity profiles, and the numerical

solutions remained stable and proceeded smoothly to a steady state for all mesh sizes considered. Inflectional profiles which satisfied Fjørtoft's criterion were found for $\alpha \geqslant 3.9$, and it was these for cases that the numerical solution became unstable.

While similar instabilities have been observed in previous studies of triple-deck flows, this appears to be the first case in which the instability is exhibited in the form of a stationary wave packet and thereby constitutes an absolute instability. The flow over a hump on the triple-deck scales is also known to be unstable (Kazakov 1985; Tutty & Cowley 1986), wherein a wave packet forms downstream of a hump of sufficient height. However, the wave packet for the hump is convected downstream after formation and therefore is referred to as a convective instability (Drazin & Reid 1981). The instability in that case was hypothesized by Tutty & Cowley (1986) to be responsible for the periodic eddy splitting observed downstream of the hump. One qualitative difference between the flow over a hump and the flow over a compression ramp is the normal location of the inflection point in the velocity profiles. The inflection point forms away from the surface in the flow over a hump, while for the compression ramp, the inflection point first forms near the surface. In addition, whereas the inflection point is always located within the reversed-flow region in the case of a compression ramp (see figure 4), it is always located in a region of positive velocity in the case of a hump. The evolution of an instability for flow over an unsteady hump, again on triple-deck scales, has also been considered by Duck (1985) and Tutty & Cowley (1986). In both studies the generation of wave packet type instabilities convecting downstream from the hump was attributed to a high-frequency instability.

The generation and evolution of convective wave packets has been considered in several studies. Gaster & Grant (1975) studied experimentally the evolution of three-dimensional wave packets generated by an acoustic pulse within the boundary layer on a flat plate. It was shown that the three-dimensional wave packet initially grows in amplitude and expands with a smooth envelope. But as it convects downstream, nonlinear effects distort and alter the smooth peaks. This was also demonstrated in the theoretical study by Ryzhov (1990). This last study, as well as the work of Ruban (1990), considered the evolution of wave packets in the framework of triple-deck theory. Additional studies (see, for example, Gaster 1982; Ryzhov & Terent'ev 1986; Terent'ev 1987; Jiang 1991 and the references therein) have sought to develop theoretical models which describe the evolution of wave packets during their linear stage of development. Whereas classical stability theory only considers the stability of particular modes, these theoretical models take into account modes having a broad range of frequencies which describe the formation of wave packets. It is believed that wave packets are a precursor to the formation of turbulent spots in the transition process from laminar to turbulent flow.

This work was supported by the Air Force Office of Scientific Research under Contract Nos. 91-0069 F49620–93-1-0130. K.W.C. was supported by a National Defense Science and Engineering Graduate Fellowship. One of us (A.I.R.) is grateful for financial support from United Technologies Research Center.

REFERENCES

ACKERET, J., FELDMANN, F. & ROTT, N. 1947 Investigations of compression shocks and boundary layers in gases moving at high speed. Translated in *Natl Adv. Comm. Aeronaut. Tech. Memo. No.* 1113 *ETH Zurich* No. 10, 1946.

ADAMSON, T. C. & MESSITER, A. F. 1980 Analysis of two-dimensional interactions between shock waves and boundary layers. *Ann. Rev. Fluid Mech.* **12**, 103–138.

ANDERSON, J. D. 1989 *Hypersonic and High Temperature Gas Dynamics.* McGraw Hill.

BROWN, S. N., CHENG, H. K. & LEE, C. J. 1990 Inviscid-viscous interaction on triple-deck scales in a hypersonic flow with strong wall cooling, *J. Fluid Mech.* **220**, 309–337.

BROWN, S. N., STEWARTSON, K. & WILLIAMS, P. G. 1975 Hypersonic self-induced separation. *Phys. Fluids* **18**, 633–639.

BURGGRAF, O. R. 1975 Asymptotic theory of separation and reattachment of a laminar boundary layer on a compression ramp. *AGARD-CP*-168, Paper No. 10.

BURGGRAF, O. R., RIZZETTA, D., WERLE, M. J. & VATSA, V. N. 1979 Effect of Reynolds number on laminar separation of a supersonic stream. *AIAA J.* **17**, 336–343.

CASSEL, K. W. 1993 The effect of interaction on boundary-layer separation and breakdown. PhD thesis Lehigh University, Bethlehem, Pennsylvania.

CASSEL, K. W., RUBAN, A. I. & WALKER, J. D. A. 1995 The influence of wall cooling on hypersonic boundary-layer separation and instability. *J. Fluid Mech.* (submitted).

CASSEL, K. W., SMITH, F. T. & WALKER, J. D. A. 1994 The onset of instability in unsteady boundary-layer separation. *J. Fluid Mech.* (submitted).

CHAPMAN, D. R., KUEHN, D. M. & LARSON, H. K. 1957 Investigation of separated flows in supersonic and subsonic streams with emphasis on the effect of transition. *NACA Tech. Note* 3869, pp. 419–460.

CHENG, H. K. 1993 Perspectives on hypersonic viscous flow research. *Ann. Rev. Fluid Mech.* **25**, 455–484.

DRAZIN, P. G. & REID, W. H. 1981 *Hydrodynamic Stability.* Cambridge University Press.

DUCK, P. W. 1985 Laminar flow over unsteady humps: the formation of waves. *J. Fluid Mech.* **160**, 465–498.

GASTER, M. 1982 Estimates of the errors incurred in various asymptotic representations of wave packets *J. Fluid Mech.* **121**, 365–377.

GASTER, M. & GRANT, I. 1975 An experimental investigation of the formation and development of a wave packet in a laminar boundary layer. *Proc. R. Soc. Lond.* A **347**, 253–269.

JIANG, F. 1991 Asymptotic evaluation of three-dimensional wave packets in parallel flows. *J. Fluid Mech.* **226**, 573–590.

KAZAKOV, V. A. 1985 Strongly implicit alternately-triangular method for solving problems of asymptotic boundary-layer theory. *USSR Comput. Maths Math. Phys.* **25**, 68–73.

KERIMBEKOV, R. M., RUBAN, A. I. & WALKER, J. D. A. 1994 Hypersonic boundary-layer separation on a cold wall, *J. Fluid Mech.* **274**, 163–195.

KOZLOVA, I. G. & MIKHAILOV, V. V. 1970 On strong viscous interaction on delta and swept wings. *Izv. Akad. Nauk SSSR, Mech. Zhid. i Gaza*, No. 6, 94–99; see also *Fluid Dyn.* **5**, 982–986.

LEWIS, J. E., KUBOTA, T. & LEES, L. 1968 Experimental investigation of supersonic laminar, two-dimensional boundary-layer separation in a compression corner with and without cooling. *AIAA J.* **6**, 7–14.

LIEPMANN, H. W. 1946 The interaction between boundary layers and shock waves in transonic flow. *J. Aeronaut. Sci.* **13**, 623–637.

LIGHTHILL, M. J. 1953 On boundary layers and upstream influence. II. Supersonic flows without separation. *Proc. R. Soc. Lond.* A **217**, 478–507.

MESSITER, A. F. 1979 Boundary layer separation, *Proc. 8th US Natl Congr. Appl. Mech.*, pp. 157–179. Western Periodicals, North Hollywood, California.

MESSITER, A. F. 1983 Boundary-layer interaction theory. *Trans. ASME* E: *J. Appl. Mech.* **50**, 1104–1113.

MIKHAILOV, V. V., NEILAND, V. YA. & SYCHEV, V. V. 1971 The theory of viscous hypersonic flow, *Ann. Rev. Fluid Mech.* **3**. 371–396.

NEILAND, V. YA 1969 On the theory of laminar boundary-layer separation in supersonic flow. *Izv. Akad. Nauk SSSR, Mech. Zhid. i Gaza*, No. 4, 53–57; see also *Fluid Dyn.* **4**, 33–35.

NEILAND, V. YA 1970 Upstream propogation of perturbations in a hypersonic flow interacting with a boundary layer. *Izv. Akad. Nauk SSSR, Mech. Zhid. i Gaza* No. 4, 40–49; see also *Fl. Dyn.* **5**, 559–566.

NEILAND, V. YA 1973 Peculiarities of boundary-layer separation on a cooled body and its interaction with a hypersonic flow. *Izv. Akad. Nauk SSSR, Mech. Zhid. i Gaza* No. 6, 99–109; see also *Fluid Dyn.* **8**, 931–939.

NEILAND, V. YA. 1974 Asymptotic problems of the viscous supersonic flow theory. *TsAGI Trans.*, No. 1529.

NEILAND, V. YA. 1981 Asymptotic theory for separation and interaction of a boundary layer with supersonic gas flow. *Adv. Mech.* **4**, No. 2, 3–62.

PERIDIER, V. J., SMITH, F. T. & WALKER, J. D. A. 1991 Vortex-induced boundary-layer separation. Part 1. The unsteady limit problem $Re \rightarrow \infty$. *J. Fluid Mech.* **232**, 99–132.

RIZZETTA, D. P., BURGGRAF, O. R. & JENSON, R. 1978 Triple-deck solutions for viscous supersonic and hypersonic flow past corners. *J. Fluid Mech.* **89**, 535–552.

RUBAN, A. I. 1978 Numerical solution of the local asymptotic problem of the unsteady separation of a laminar boundary layer in a supersonic flow. *USSR Comput. Maths Math. Phys.* **18**, 175–187.

RUBAN, A. I. 1990 Propagation of wave packets in the boundary layer on a curved surface. *Izv. Akad. Nauk SSSR, Mech. Zhid. i Gaza* No. 2, 59–68; see also *Fluid Dyn.* **25**, 213–221.

RYZHOV, O. S. 1990 The formation of ordered vortex structures from unstable oscillations in the boundary layer *USSR Comput. Maths. Math. Phys.* **30**, 146–154.

RYZHOV, O. S. & TERENT'EV, E. D. 1986 On the transition regime characterizing the start of a vibrator in subsonic boundary layer on a flat plate. *Appl. Math. Mech.* **50**, 974–986.

SMITH, F. T. 1982 On the high Reynolds number theory of laminar flows. *IMA J. Appl. Maths* **28** 207–281.

SMITH, F. T. 1988 A reversed-flow singularity in interacting boundary layers. *Proc. R. Soc. Lond.* A **420**, 21–52.

SMITH, F. T. & KHORRAMI, A. F. 1991 The interactive breakdown in supersonic ramp flow. *J. Fluid Mech.* **224**, 197–215.

SMITH, F. T., SYKES, R. I. & BRIGHTON, P. W. M. 1977 A two-dimensional boundary layer encountering a three-dimensional hump. *J. Fluid Mech.* **83**, 163–176.

STEWARTSON, K. 1964 *Boundary Layers in Compressible Flow.* Oxford University Press.

STEWARTSON, K. 1974 Multistructured boundary layers on flat plates and related bodies. *Adv. Appl. Mech.* **14**, 145–239.

STEWARTSON, K. 1981 D'Alembert's Paradox. *SIAM Rev.* **23**, 308–343.

STEWARTSON, K. & WILLIAMS, P. G. 1969 Self-induced separation. *Proc. R. Soc. Lond.* A **312**, 181–206.

TERENT'EV, E. D. 1987 On the formation of wave packet in the boundary layer on a flat plate. *Appl. Math. Mech.* **51**, 814–819.

TUTTY, O. R. & COWLEY, S. J. 1986 On the stability and the numerical solution of the unsteady interactive boundary-layer separation. *J. Fluid Mech.* **168**, 431–456.